

Entangled collective spin states of two-species ultracold atoms in a ringTomáš Opatrný¹ and Kunal K. Das^{2,3}¹*Department of Optics, Palacký University, 771 46 Olomouc, Czech Republic*²*Department of Physical Sciences, Kutztown University of Pennsylvania, Kutztown, Pennsylvania 19530, USA*³*Department of Physics and Astronomy, Stony Brook University, Stony Brook, New York 11794, USA*

(Received 16 March 2023; revised 9 August 2023; accepted 29 September 2023; published 18 October 2023)

Two species of mutually interacting ultracold bosonic atoms are studied in a ring-shaped trap with a species-selective azimuthal lattice which may rotate. We examine the spectrum and the states in a collective spin formalism. The system can be modeled as a pair of coupled Lipkin-Meshkov-Glick Hamiltonians, and can be used to generate a high degree of entanglement. The Hamiltonian has two components: a linear part that can be controlled by manipulating the azimuthal lattice, and an interaction-dependent quadratic part. Exact solutions are found for the quadratic part for equal strengths of intraspecies and interspecies interactions. In different regimes the Hamiltonian can emulate a beam splitter or a two-mode squeezer of quantum optical systems. We study entanglement properties of the ground state of the Hamiltonian in dependence on various parameters with the prospect of possible quantum information and metrology applications.

DOI: [10.1103/PhysRevA.108.043307](https://doi.org/10.1103/PhysRevA.108.043307)**I. INTRODUCTION**

The coherent state in a closed loop is a defining paradigm of quantum mechanics, tracing back to de Broglie's explanation of quantization of electronic states in atoms [1]. With the creation of coherence in many-body systems, such as with Bose-Einstein condensates (BECs), and progress in trapping them in toroidal configurations, that seminal configuration can be translated to macroscopic scales. The closed topology and the natural superfluidity associated with degenerate cold gases have focused most of the interest in this matter on the physics of persistent flows [2,3]. However, the coherent flow in a loop intrinsically comes with angular momentum, and with the circulating modes parallels can be drawn with states of electrons within atoms, including spin and orbital momenta [4]. The many-body nature [5] of such macroscopic coherent media and rich nonlinear behavior due to interactions [6] means that such ring systems can be a versatile simulator of collective spin states [7] and the rich physics associated with them. This paper aims to explore the features of entanglement generated in such systems.

Multiple pathways exist for creating ring traps for atoms [2,8–16], some conveniently adaptable to include azimuthal lattice structures, such as the use of Laguerre-Gaussian beams [17,18]. While numerous experiments [3,19,20] have been conducted with cold atoms in ring traps, proportionate efforts with the inclusion of lattices are overdue, notwithstanding the rich physics indicated by continuing theoretical works [21–36].

In previous work, we have shown that a single species in a ring can lead to rich physics: The dynamics can display coherent oscillations between various modes coupled by a lattice [4], nonlinear dynamical behavior like self-trapping is evident [6,36], and creation of spin squeezed states and simulation of Lipkin-Meshkov-Glick dynamics are possible [35,37]. However, to examine quantum correlations associated with multi-particle entanglement [38] that touch on the most intriguing

aspects of quantum mechanics, such as Einstein-Podolsky-Rosen and Bell inequalities, that analog in a ring is best implemented with two species of atoms. Simulation of such intrinsically quantum phenomena with the macroscopic states of a ring motivates this paper. The common collective spin description also allows for analogous macroscopic realizations of nonclassical states of collective atomic spins for applications in metrology [39,40] and for quantum computation [41]. Here, we focus on the spectrum and the degree of entanglement of the relevant quantum states in the system, preliminary to examining the dynamics in our continuing work.

In Sec. II, we describe our system and derive the two-species Hamiltonian, and transform it to a collective spin description; subsequently in Sec. III we provide physical interpretation of the various features of the model and justify some of the assumptions we make in our analysis. We set up the states and the measure of entanglement for the system in Sec. IV. Then in Sec. V, we derive analytical expressions for the eigenvalues and for the associated states for the quadratic Hamiltonian that creates entanglement, and we consider various special cases. Section VI highlights limiting cases where the system behavior is analogous to a beam splitter and a spin squeezer in turn. In Sec. VII, the density of states for the full Hamiltonian is shown to display features of a phase transition as the Hamiltonian is continuously changed from the linear limit to the quadratic limit. In Sec. VIII, we present analysis and estimates, using parameters based on existing technologies, to demonstrate feasibility of implementation of our model in experiments. We conclude in Sec. IX with a discussion of the broader relevance and with an outlook of our ongoing work on dynamical applications of these results.

II. SYSTEM AND MODEL

We consider two species of BEC composed of N_1 and N_2 atoms in a toroidal trap as shown in Fig. 1. The variables for the two species will be indexed by subscripts $i = 1, 2$. We take

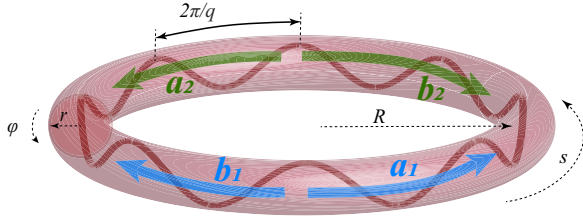


FIG. 1. Two species of atoms labeled $i = 1, 2$ are trapped in a toroidal trap with the option of an azimuthal lattice potential of period $2\pi/q$. The two lowest counterpropagating modes for each species are denoted by letters a and b . The torus is taken as a wrapped cylinder with our choice of coordinates $\mathbf{r} = (s, r, \varphi)$ shown.

the minor radius r of the torus to be much smaller than its major radius R so that the system can be treated as a cylinder $\mathbf{r} = (s, r, \varphi)$ with periodic boundary condition on the circumferential coordinate s . We assume the confinement along (r, φ) transverse to the ring circumference to be sufficiently strong to keep the atoms in the ground state $\psi_i(r, \varphi)$ for those degrees of freedom, so that the three-dimensional bosonic field operator can be written in the factorized form $\hat{\Psi}_i(s)\psi_i(r, \varphi)$. Integrating over the transverse degrees of freedom yields an effective one-dimensional (1D) Hamiltonian:

$$\hat{H} = \int_0^{2\pi R} ds \left[\sum_{i=1,2} \hat{\Psi}_i^\dagger \left(-\frac{\hbar^2}{2m_i} \partial_s^2 + U_i + \frac{g_i}{4\pi l_i^2} \hat{\Psi}_i^\dagger \hat{\Psi}_i \right) \hat{\Psi}_i + \frac{g_{12}}{2\pi l_{12}^2} \hat{\Psi}_1^\dagger \hat{\Psi}_2^\dagger \hat{\Psi}_1 \hat{\Psi}_2 \right] \quad (1)$$

where $g_\alpha = 4\pi \hbar^2 a_\alpha / m_\alpha$ is the interaction strength defined by the s -wave scattering length a_α , with $\alpha \in \{1, 2, 12\}$, and l_i is the harmonic oscillator length for the transverse confinement for the two species. The interspecies counterparts are

$$\begin{aligned} \hat{H} = & \sum_n (\hbar\omega_n - \hbar n\Omega) (\hat{c}_{1n}^\dagger \hat{c}_{1n} + \hat{c}_{2n}^\dagger \hat{c}_{2n}) + \frac{1}{2} \hbar \sum_{\substack{n,m,k,p \\ n+m-k-p=0}} [\chi_1 \hat{c}_{1n}^\dagger \hat{c}_{1m}^\dagger \hat{c}_{1k} \hat{c}_{1p} + \chi_2 \hat{c}_{2n}^\dagger \hat{c}_{2m}^\dagger \hat{c}_{2k} \hat{c}_{2p} + 2\chi_{12} \hat{c}_{1n}^\dagger \hat{c}_{2m}^\dagger \hat{c}_{1k} \hat{c}_{2p}] \\ & + \sum_n \hbar [u_{1-} \hat{c}_{1n}^\dagger \hat{c}_{1(n-2q)} + u_{1+} \hat{c}_{1n}^\dagger \hat{c}_{1(n+2q)}] + \sum_n \hbar [u_{2-} \hat{c}_{2n}^\dagger \hat{c}_{2(n-2q)} + u_{2+} \hat{c}_{2n}^\dagger \hat{c}_{2(n+2q)}]. \end{aligned} \quad (5)$$

Here eigenenergies associated with the circulating modes of the ring are $\hbar\omega_n = \frac{\hbar^2 n^2}{2mR^2}$, and we have defined the effective 1D interaction strengths $\chi_\alpha = \frac{g_\alpha}{4\hbar\pi^2 l_\alpha^2 R}$ and the linear combination of the lattice depths $u_{i\pm} = \frac{1}{2}(u_{xi} \pm iu_{yi})$. Note, we put a parentheses around $(n \pm 2q)$ to indicate that the “2” inside is a multiplicative factor and not a species index unlike the other numerical subscripts.

At this point, we assume that the ring is sufficiently small and the density low enough such that the energy gaps $\hbar\omega_n$ are large compared to the energy scale of the interatomic interactions $\chi_\alpha N_\alpha / (2\pi R)$, where $N_{12} = \sqrt{N_1 N_2}$. This means the interaction will not significantly couple modes with different

$l_{12} = \sqrt{l_1 l_2}$ and the reduced mass of the two species $m_{12} = m_1 m_2 / (m_1 + m_2)$.

The potential along the ring is taken to be a periodic lattice. Assuming species selective lattice potential we allow for different strengths for the potentials U_i experienced by each species. However, we assume the same rate of rotation for both, which will allow us to treat the Hamiltonian as stationary:

$$U_i(s, t) = \hbar u_{xi} \cos \left[2q \left(\frac{s}{R} - \Omega t \right) \right] + \hbar u_{yi} \sin \left[2q \left(\frac{s}{R} - \Omega t \right) \right]. \quad (2)$$

We have allowed for two lattices, one symmetric (x) and one antisymmetric (y) relative to the coordinate origin. This allows for a general formalism in terms of collective spin operators.

We can eliminate the explicit dependence on the time in the Hamiltonian, by transforming to a frame rotating with the lattice. This transforms the potential to have arguments $\frac{s}{R} - \Omega t \rightarrow \frac{s}{R}$, but adds an angular momentum term to the Hamiltonian:

$$\hat{H} \rightarrow \hat{H} + i\hbar\Omega \int_0^{2\pi R} ds \hat{\Psi}_i^\dagger \partial_s \hat{\Psi}_i. \quad (3)$$

We now expand the field operator in the eigenstates of the ring:

$$\hat{\Psi}_i(s) = \sum_n \hat{c}_{in} \psi_n(s), \quad \psi_n(z) = \frac{1}{\sqrt{2\pi R}} e^{in(s/R)}, \quad (4)$$

where the field amplitudes \hat{c}_{in} for the modes for each species satisfy the bosonic commutator rules $[\hat{c}_{in}, \hat{c}_{jm}] = \delta_{ij} \delta_{mn}$. The first index is the species index while the second index is the mode index. Thereby, we can write the *time-independent* Hamiltonian in the *rotating* frame as

energies. We therefore consider two degenerate modes that match the lattice periodicity $n = \pm q$ in Eq. (4), that is, $e^{\pm iqs/R}$. Then in the nonlinear terms, if we set the indices $n, m, k = \pm q$ the fourth index $p = \pm q$ and $\pm 3q$. Likewise the lattice also couples $\pm q$ and $\pm 3q$, but we assume a weak lattice that only couples mutually degenerate modes. Therefore, we will neglect the coupling to the $\pm 3q$ and consider only the subspace of two modes $\pm q$. We have previously shown [36] that, for experimentally feasible parameters, single species dynamics justifies this assumption, with negligible loss of population from the two-mode subspace as the system evolved. By focusing on the two-mode subspace, we can remove the modal

summation in Eq. (5) and have the effective Hamiltonian

$$\begin{aligned} \hat{H}_{\text{eff}} = & \sum_{i=1,2} [-\hbar q \Omega (\hat{a}_i^\dagger \hat{a}_i - \hat{b}_i^\dagger \hat{b}_i) + \hbar (u_{i-} \hat{a}_i^\dagger \hat{b}_i + u_{i+} \hat{b}_i^\dagger \hat{a}_i)] \\ & + \frac{1}{2} \hbar \chi_i (\hat{a}_i^\dagger \hat{a}_i^\dagger \hat{a}_i \hat{a}_i + 4 \hat{a}_i^\dagger \hat{b}_i^\dagger \hat{a}_i \hat{b}_i + \hat{b}_i^\dagger \hat{b}_i^\dagger \hat{b}_i \hat{b}_i) \\ & \times \hbar \chi_{12} [\hat{a}_1^\dagger \hat{a}_2^\dagger \hat{a}_1 \hat{a}_2 + \hat{a}_1^\dagger \hat{b}_2^\dagger \hat{a}_1 \hat{b}_2 + \hat{a}_1^\dagger \hat{b}_2^\dagger \hat{b}_1 \hat{a}_2 \\ & + \hat{b}_1^\dagger \hat{a}_2^\dagger \hat{a}_1 \hat{b}_2 + \hat{b}_1^\dagger \hat{a}_2^\dagger \hat{b}_1 \hat{a}_2 + \hat{b}_1^\dagger \hat{b}_2^\dagger \hat{b}_1 \hat{b}_2]. \end{aligned} \quad (6)$$

Here we have set $\hbar \omega_q = 0$ as the energy reference and we relabeled the operators for the $\pm q$ modes for each species $\hat{c}_{i(n=+q)} = \hat{a}_i$ and $\hat{c}_{i(n=-q)} = \hat{b}_i$ respectively. The terms in the Hamiltonian have ready physical interpretation: As regards the linear terms, the lattice couples counterpropagating modes of the same species, while the rotation shifts the relative energies of modes. The nonlinear terms describe the mutual scattering of two modes of the same species or of different species.

In order to continue the analysis, we recast the Hamiltonian in terms of the collective spin operators

$$\begin{aligned} \hat{J}_{xi} & \equiv \frac{1}{2} (\hat{a}_i^\dagger \hat{b}_i + \hat{a}_i \hat{b}_i^\dagger), \\ \hat{J}_{yi} & \equiv \frac{1}{2i} (\hat{a}_i^\dagger \hat{b}_i - \hat{a}_i \hat{b}_i^\dagger), \\ \hat{J}_{zi} & \equiv \frac{1}{2} (\hat{a}_i^\dagger \hat{a}_i - \hat{b}_i^\dagger \hat{b}_i), \end{aligned} \quad (7)$$

so that the Hamiltonian takes the form

$$\begin{aligned} \hat{H}_{\text{eff}} = & \sum_{i=1,2} [-2\hbar q \Omega \hat{J}_{zi} + \hbar u_{xi} \hat{J}_{xi} + \hbar u_{yi} \hat{J}_{yi}] \\ & + \hbar \sum_{i=1,2} \chi_i [\hat{J}_{xi}^2 + \hat{J}_{yi}^2] + 2\hbar \chi_{12} [\hat{J}_{x1} \hat{J}_{x2} + \hat{J}_{y1} \hat{J}_{y2}] \end{aligned} \quad (8)$$

where some constant terms have been left out taking into account that $\hat{J}_{xi}^2 + \hat{J}_{yi}^2 + \hat{J}_{zi}^2 = \frac{N_i}{2} (\frac{N_i}{2} + 1)$ commute with the Hamiltonian and do not influence the dynamics. For each species separately, the linear terms together with the self-interaction quadratic terms form a generalized version of the so called Lipkin-Meshkov-Glick (LMG) Hamiltonian that was originally introduced to model particular systems in nuclear physics [37], but later found application in many other branches of physics. For collective spins, the quadratic part corresponds to the one-axis-twisting dynamics proposed by Kitagawa and Ueda [7] that was used to generate spin squeezing in cold atomic samples [39,40]. We have studied the LMG dynamics in ring traps with bosons in our previous work [35,36]. The bilinear terms proportional to χ_{12} containing the cross terms $\hat{J}_{x1} \hat{J}_{x2} + \hat{J}_{y1} \hat{J}_{y2}$ are new and represent a further generalization of the LMG model to two coupled LMG systems. Although similar coupling of two collective spin samples through an interaction $\hat{J}_{z1} \hat{J}_{z2}$ has been proposed for trapped atoms inside coupled optical resonators by one of us [41], the interspecies coupling in Eq. (8) for orbital or external degree of freedom has not been previously explored and will be in the center of further considerations in this paper.

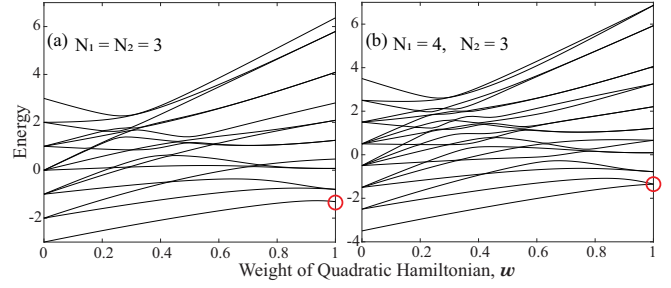


FIG. 2. [(a), (b)] The eigenvalues of the Hamiltonian in Eq. (8) are plotted as the weight w of the quadratic Hamiltonian is varied from the linear limit to the quadratic limit. In the quadratic limit the ground state, marked by a red circle, is (a) nondegenerate when $N_1 = N_2$ and (b) degenerate when $N_1 \neq N_2$; this is true even for different values for the interaction strengths as used here, $\chi_1 = 1$, $\chi_2 = 1.5$, and $\chi_{12} = 2$. In the linear limit, we use $\hat{H}_L = (\hat{J}_{x1} - \hat{J}_{x2})$ in Eq. (8), corresponding to an azimuthal lattice with no rotation.

III. PHYSICAL PICTURE AND ASSUMPTIONS

The linear part of the Hamiltonian in Eq. (8) generates rotations of the Bloch spheres of the two species. It can be controlled and even completely turned off with the lattice strength and the rotation Ω . Whereas the rotations around the J_x and J_y can be performed independently for the two species, rotation around the J_z axis is common and governed by the physical rotation of the system. Nevertheless, this does not inhibit the option to achieve independent rotations around J_{zi} by sequences of switching on and off the u_{xi} and u_{yi} lattices, realizing the Trotter sequence of $J_{zi} = i(J_{yi} J_{xi} - J_{xi} J_{yi})$ (see for example in Ref. [42]). The quadratic part can be likewise controlled or made to vanish with the interaction induced nonlinearity.

In an experiment, it would be convenient to initialize the system in the ground state of the linear Hamiltonian and adiabatically transition to the ground state of the quadratic Hamiltonian. For example, we can start with $\Omega = 0$, a static lattice, and choose $u_{y1} = u_{y2} = 0$ and parametrize the non-vanishing amplitudes by $u_{x1} = -u_{x2} = 1 - w$. Then we can write the Hamiltonian as $(1 - w)\hat{H}_L + w\hat{H}_Q$, with a linear part $\hat{H}_L = \hat{J}_{x1} - \hat{J}_{x2}$ and a quadratic part \hat{H}_Q defined as in the second line of Eq. (8), with $\chi_\alpha \rightarrow \chi_\alpha/w$. Physically this choice means that in the limit of only linear interaction, the two species have ground states that are standing waves that avoid each other (on the corresponding Bloch spheres, on the equator but on opposite sides). Adiabatic transition from the linear to the quadratic regime would then keep the system in the ground state with the two species avoiding each other, and arrive at the maximally entangled state analogous to the singlet state of two particles.

It is implicit that the nonlinear strengths χ_α change proportionately to w ; in practice, that can be accomplished by any number of ways, such as tuning close to Feshbach resonances or reducing density, creating relative displacement of the two species, or by adjusting the transverse confinement. The parameter w therefore serves as a measure of the relative strengths of the linear and the quadratic part, and we plot the variation of the spectrum as a function of this parameter in Fig. 2. In order to maintain comparable scales, the quadratic

part is scaled in the figure by the average particle number $\hat{H}_Q \rightarrow 2\hat{H}_Q/(N_1 + N_2)$.

The ground state is found to have two distinct behaviors. For $N_1 = N_2$, the ground state remains nondegenerate from purely linear to purely quadratic, whereas for $N_1 \neq N_2$ at the quadratic limit the ground state is always double degenerate. However, when the linear limit has copropagating modes in the two species, the gap may close before reaching the quadratic limit. Still, the state can be initially prepared to sustain the gap so that almost total adiabatic transfer can be achieved from the ground state of the linear Hamiltonian to that of the quadratic Hamiltonian for systems with equal number of particles of both species.

If the intra- and interspecies couplings are identical, $\chi_1 = \chi_2 = \chi_{12} = \chi$, which can be true to a good approximation for example for ^{87}Rb atoms [43], we can express the Hamiltonian as the sum of linear and quadratic parts $\hat{H} = \hat{H}_L + \hat{H}_Q$:

$$\begin{aligned} \hat{H}_L &= \sum_{i=1,2} [-2q\Omega\hat{J}_{zi} + u_{xi}\hat{J}_{xi} + u_{yi}\hat{J}_{yi}], \\ \hat{H}_Q &= \chi(\hat{J}_{x1} + \hat{J}_{x2})^2 + \chi(\hat{J}_{y1} + \hat{J}_{y2})^2. \end{aligned} \quad (9)$$

This form assumes units to be used in all our numerical simulations; *we will take the major radius R as the length unit, energy of the lowest circulating mode $\hbar\omega_1 = \frac{\hbar^2}{2mR^2}$ as the energy unit, and associated frequency ω_1 as the frequency unit.*

We define the collective operators $\hat{J}_{p\pm} = \hat{J}_{p1} \pm \hat{J}_{p2}$, with $p \in \{x, y, z\}$ so the quadratic part simply becomes $\hat{H}_Q = \hat{J}_{x+}^2 + \hat{J}_{y+}^2$. The quadratic part is of more significance because it changes the shape of the states, and we will focus on that. In addition to N_1 and N_2 , the quadratic part also clearly commutes with $\hat{J}_{z\pm} \equiv \hat{J}_{z1} + \hat{J}_{z2}$. In the rest of the paper when we primarily focus on the quadratic Hamiltonian, without loss of generality, *we set $\chi = 1$* , which would simply imply a rescaling of the energy units.

IV. STATES AND ENTANGLEMENT ENTROPY

The system can be described in Fock basis, that specifies the occupation of each of the four modes $|n_{a1}, n_{b1}\rangle \otimes |n_{a2}, n_{b2}\rangle$. More specifically, we can write the basis as a direct product of Dicke states, the collective spin analog of Fock states, of the two species $|j_1, m_1\rangle \otimes |j_2, m_2\rangle$. For fixed particle number, we have $j_i = N_i/2$. The second quantum number specifies eigenstates of

$$\hat{J}_{zi}|j_i, m_i\rangle = m_i|j_i, m_i\rangle, \quad m_i = -\frac{N_i}{2}, -\frac{N_i}{2} + 1, \dots, \frac{N_i}{2}. \quad (10)$$

We can further simplify to a basis of eigenstates of $\hat{J}_{z\pm}$ that we denote by

$$\hat{J}_{z\pm}|z_+, z_-\rangle = z_{\pm}|z_+, z_-\rangle. \quad (11)$$

Since z_+ is a conserved quantum number for the quadratic part of the Hamiltonian in Eq. (8), we can consider subspaces of fixed z_+ independently within which the states are uniquely labeled by a single quantum number z_- :

$$\begin{aligned} n_{a1} &= \frac{1}{2}(N_1 + z_+ + z_-), \\ n_{b1} &= \frac{1}{2}(N_1 - z_+ - z_-), \end{aligned}$$

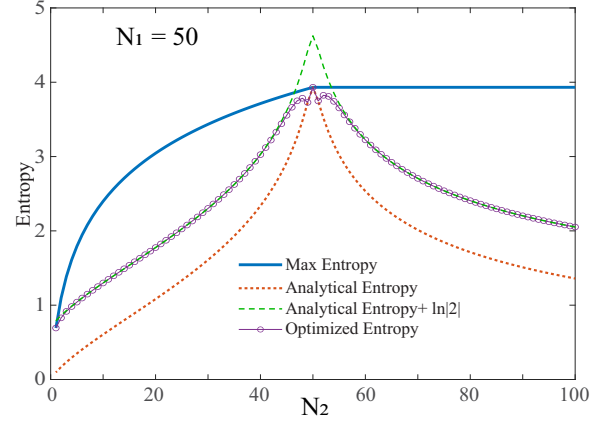


FIG. 3. The effect of imbalance in particle number of the two species is illustrated for the ground state of the quadratic Hamiltonian \hat{H}_Q , by plotting the associated entropy of entanglement as a function of particle number N_2 of the second species, with that of the first one fixed at $N_1 = 50$. The maximum entropy is set by that of the lower particle count. The dotted red line is computed analytically from the exact ground state in Eq. (18); the dashed green line has $\ln|2|$ added to account for the twofold degeneracy, which however is an overestimate close to $N_1 = N_2$. The circle markers are numerical calculations for an optimal superposition of the degenerate states in Eq. (18).

$$\begin{aligned} n_{a2} &= \frac{1}{2}(N_2 + z_+ - z_-), \\ n_{b2} &= \frac{1}{2}(N_2 - z_+ + z_-). \end{aligned} \quad (12)$$

The density matrix ρ corresponding to the ground state of the quadratic Hamiltonian of the composite system can be expressed in this basis. We measure the degree of entanglement between the two species by computing the von Neumann entanglement entropy [44] using the reduced density matrix $\rho_2 = \text{Tr}_1(\rho)$ or $\rho_1 = \text{Tr}_2(\rho)$:

$$S(\rho_2) = -\text{Tr}[\rho_2 \ln(\rho_2)] = -\sum_i [\epsilon_i \ln(\epsilon_i)]. \quad (13)$$

The last step follows from assuming the density matrix can be diagonalized and ϵ_i are its eigenvalues. The entropy is not sensitive to the choice of the reduced density matrix $S(\rho_1) = S(\rho_2)$.

We compute the variations of the entropy with respect to the imbalance of the particle number and present them in Fig. 3. This underscores another advantage of a system of equal number of particles in both species. The entropy is maximized when $N_1 = N_2$, as shown for two separate values of N_1 fixed as N_2 is varied. The maximum entropy is set by the smaller particle number $S_{\max} = \ln |\min(N_1, N_2)|$. The entanglement entropy is computed analytically from the solution that appears in Eq. (18) in the next section. An inherent degeneracy present in the ground state for unequal particle number underestimates the entropy for any specific ground state. We correct for this by adding $\ln|2|$ to allow for the degeneracy. When the imbalance is high, we find this matches almost exactly the numerically computed entropy that optimizes for the linear combination of the degenerate ground states, suggesting equal weight maximizes the entropy. However, close to equal

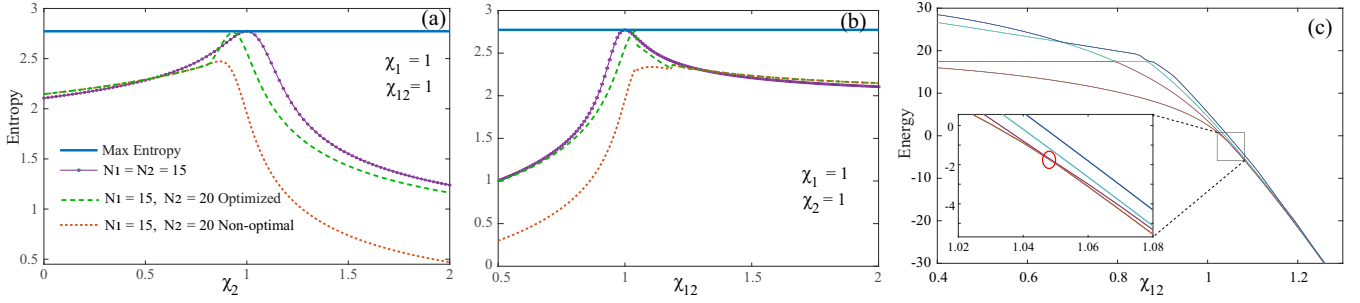


FIG. 4. The entanglement entropy of the ground state of the quadratic Hamiltonian is seen to be maximized when all the interaction strengths are the same, $\chi_1 = \chi_2 = \chi_{12}$, as assumed in Eq. (9). (a) The rate of decline with deviation from that is faster at (a) larger values of an intraspecies χ_2 and (b) smaller values of interspecies interactions χ_{12} . For $N_1 \neq N_2$ optimizing the superposition (green dashed line) can raise the entanglement entropy to be almost the same as for equal particle numbers (solid purple line with markers). (c) Degeneracies in the spectrum, that mark crossing of spectral lines that include the ground state, coincide with discontinuous jumps in the entropy, shown here for an example in panel (b).

number of particles, addition of $\ln |2|$ generally overestimates the entropy and the optimal entropy is not necessarily an equal weight combination of the degenerate analytical solutions.

In Fig. 4, we probe the sensitivity to our assumption of equal interaction strengths, by plotting the entanglement entropy as we vary one of χ_α keeping the other two fixed. When we vary χ_2 keeping χ_1 and χ_{12} fixed, for both equal and unequal number of atoms, we find as seen in panel (a) the entropy decreases faster when χ_2 is larger. On the other hand when we vary χ_{12} with the other two fixed, panel (b) shows that the entropy drops off faster when χ_{12} is larger. Therefore we can conclude that if there is a difference in the interaction strengths, it is better to have the interspecies interaction to be stronger than the intraspecies ones. The numerical computation of the entropy occasionally displays discontinuous jumps. We illustrate in Fig. 4(c) that those jumps correspond to degeneracies where the ground state changes identity due to different spectral lines crossing.

V. ANALYTICAL EIGENVALUES AND STATES

In the case of all the couplings being the same, the quadratic Hamiltonian \hat{H}_Q in Eq. (9) can be diagonalized exactly. In the basis $|z_+, z_-\rangle$ defined above the Hamiltonian acquires a block-tridiagonal structure:

$$\begin{aligned} \hat{H}_Q |z_+, z_-\rangle &= (n_{a1}n_{b1} + n_{a2}n_{b2} - \frac{1}{2}N) |z_+, z_-\rangle \\ &+ \sqrt{n_{a1}(n_{b1} + 2)(n_{a2} + 2)n_{b2}} |z_+, z_- - 2\rangle \\ &+ \sqrt{(n_{a1} + 2)n_{b1}n_{a2}(n_{b2} + 2)} |z_+, z_- + 2\rangle, \end{aligned} \quad (14)$$

where the n_i are given by Eq. (12), and we define the total particle number $N = N_1 + N_2$. Each block of fixed z_+ has tridiagonal form comprising a set by the allowed z_- values. We determine the eigenvalues to be given by

$$\begin{aligned} E_n &= n(n + 1) + |z_+|(2n + 1), \\ z_+ &= 0, \pm 1, \pm 2, \dots \pm \frac{1}{2}N \quad \text{even } N, \\ z_+ &= \pm \frac{1}{2}, \pm \frac{3}{2}, \dots \pm \frac{1}{2}N \quad \text{odd } N \end{aligned} \quad (15)$$

where $n \in \{n_{\min}, n_{\min} + 2, \dots, n_{\max}\}$, with

$$\begin{aligned} n_{\min} &= \max\left(\frac{1}{2}|N_2 - N_1| - |z_+|, 0\right), \\ n_{\max} &= \frac{1}{2}N - |z_+|. \end{aligned} \quad (16)$$

This confirms explicitly some of the conclusions of the numerical results displayed in Fig. 2: When $N_1 = N_2$, the expressions above show that the ground state is indeed unique corresponding to $z_+ = 0$, $n = 0$, and energy $E_0 = 0$. But, when $N_1 \neq N_2$, the lowest-energy state is doubly degenerate, corresponding to $n = 0$, but with

$$z_+ = \pm \frac{N_1 - N_2}{2}, \quad E_0 = \frac{|N_1 - N_2|}{2}. \quad (17)$$

The eigenvalues depend on the atomic numbers $N_{1,2}$ only through the limits for the index n , as illustrated in Fig. 5. Since all the eigenvalues are integers or semi-integers with their smallest nonzero difference being 1, the evolution of any state is periodic with period 2π , assuring periodic behavior. This contrasts with a semiclassical description that will be reported in an upcoming work which suggests that the period should go to infinity.

Without loss of generality, we assume $N_1 \leq N_2$, and the ground state for arbitrary particle numbers for the two species can be expressed in terms of the basis states $|z_+, z_-\rangle$ as

$$\begin{aligned} |\psi_{0,\pm}\rangle &= \sum_{k=0}^{N_1} \alpha_k \left| \pm \frac{1}{2}(N_2 - N_1), \mp \left[\frac{1}{2}(N_2 - 3N_1) + 2k \right] \right\rangle, \\ \frac{\alpha_k}{\alpha_{k-1}} &= -\sqrt{\frac{N_2 - N_1 + k}{k}}, \end{aligned} \quad (18)$$

where the coefficients α_k are defined recursively. This formula also covers the special case $N_1 = N_2 = \frac{1}{2}N$, when the ground state becomes nondegenerate, with energy $E_0 = 0$ and $z_+ = 0$. The expressions then reduce to a simpler form which can be written as a superposition of states $|z_-\rangle$:

$$|\psi_0\rangle = \frac{\sqrt{2}}{\sqrt{N}} \sum_{k=0}^{\frac{1}{2}N} (-1)^k \left| -\frac{1}{2}N + 2k \right\rangle. \quad (19)$$

Beyond the ground state, in the special case of equal number of particles, $N_1 = N_2 = \frac{1}{2}N$, and in the subspace of $z_+ =$

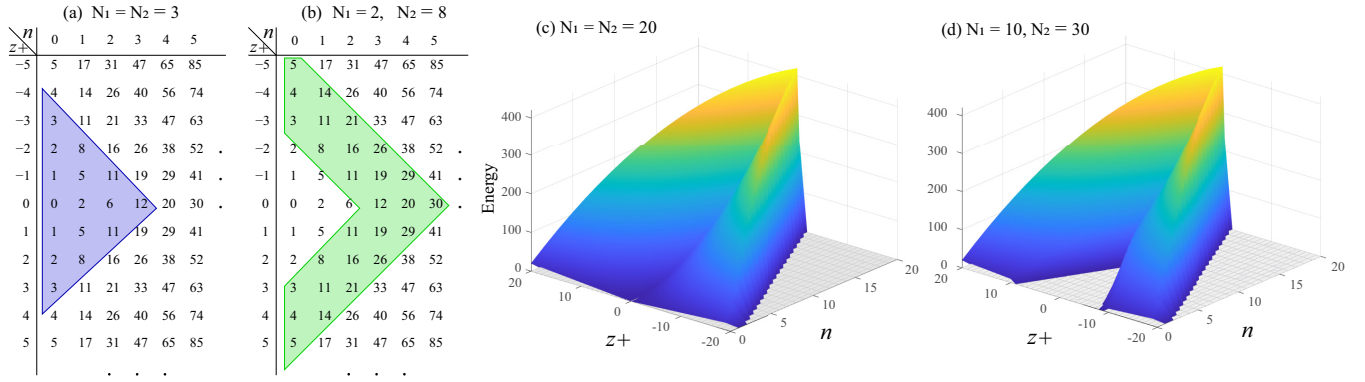


FIG. 5. The eigenvalues of \hat{H}_Q are shown in the space of z_+ and n . The allowed eigenvalues are shown by colored shading. (a) For $N_1 = N_2$, for any allowed z_+ the minimum value of z_- is always zero. (b) For $N_1 \neq N_2$, there is a regime of the lower $|z_-|$ where the lowest natural numbers including zero are excluded, creating a boomerang shape. The energy is plotted as a function of z_+ and n for (c) equal particle number $N_1 = N_2$, when there is no gap at $n = 0$, and for (d) unequal particle number $N_1 \neq N_2$ when a gap emerges for lower z_+ values.

0, which means there is an equal number of counterpropagating atoms as well, the energy is simply $E_n = n(n+1)$ and the complete set of states in the subspace is given by

$$|z_-\rangle = \left| -\frac{1}{2}N + 2n \right\rangle, \quad n \in \{0, 1, \dots, \frac{1}{2}N\}. \quad (20)$$

This has an interesting implication for the dynamics. Since now all the eigenvalues are even integers and the minimum-energy difference is 2, the evolution of any state is periodic with half the period compared to the more general case above, where the level spacing is unity as seen Eq. (15)

For *minimal* asymmetry, $N_2 = N_1 + 1$, the ground states have energy $E_0 = \frac{1}{2}$ and correspond to $z_+ = \pm\frac{1}{2}$. Expressed as superpositions of states $|z_+, z_-\rangle$ they are

$$|\psi_{0,\pm}\rangle = \frac{\sqrt{2}}{\sqrt{N(N+1)}} \sum_{k=0}^{N_1} (-1)^k \sqrt{k+1} \times \left| \pm\frac{1}{2}, \pm\left(N_1 - \frac{1}{2} - 2k\right) \right\rangle. \quad (21)$$

We conclude the section with an intuitive picture of the reason for the degeneracy of the ground state when particle numbers are different. With equal particle numbers there are complete pairs of counterpropagating modes, with unequal numbers there can be unbalanced modes, but in the absence of rotation both orientations of rotation have identical energies leading to a degeneracy. There can be interesting dynamical effects of the degeneracy; for example, if the system is prepared in the ground state of the linear Hamiltonian as in Fig. 2(b), adiabatic change $w = 0$ to 1 to the completely nonlinear regime and back again to the linear regime can result in superposition of the lowest pair of states that happen to degenerate when $w = 1$.

VI. LIMITING CASES

We now underscore the broad relevance of this Hamiltonian by identifying some limiting cases for the quadratic part \hat{H}_Q . For this purpose, it is more transparent to express it in terms of the creation and annihilation operators:

$$\hat{H}_Q = \hat{a}_1^\dagger \hat{a}_1 \hat{b}_1^\dagger \hat{b}_1 + \hat{a}_2^\dagger \hat{a}_2 \hat{b}_2^\dagger \hat{b}_2 + \frac{1}{2}(N_1 + N_2) + \hat{a}_1 \hat{b}_1^\dagger \hat{a}_2^\dagger \hat{b}_2 + \hat{a}_1^\dagger \hat{b}_1 \hat{a}_2 \hat{b}_2^\dagger. \quad (22)$$

A. Beam splitter limit

If almost all the atoms in both species are circulating in the same direction, such that b modes $b_1 \approx b_1^\dagger \approx \sqrt{N_1}$ and $b_2 \approx b_2^\dagger \approx \sqrt{N_2}$, then the Hamiltonian reduces to

$$\hat{H}_Q \approx N_1 \hat{a}_1^\dagger \hat{a}_1 + N_2 \hat{a}_2^\dagger \hat{a}_2 + \frac{1}{2}(N_1 + N_2) + \sqrt{N_1 N_2} (\hat{a}_1 \hat{a}_2^\dagger + \hat{a}_1^\dagger \hat{a}_2). \quad (23)$$

The last term corresponds to a beam splitter (or linear coupler) which destroys one quantum (photon, for optical implementation) in one mode while creating one quantum in another mode (for details of the transformation, see, e.g., Ref. [45]). The first two terms are responsible for the time-dependent change of phase in the two modes, the prefactors $N_{1,2}$ playing the role of frequencies of the modes. For $N_1 = N_2 \equiv N$ (matched frequencies) the Hamiltonian leads to oscillations of the mode occupations with period π/N so that for time equal to $\pi/(2N)$ the atomic states are exchanged and for time equal to $\pi/(4N)$ the transformation corresponds to a 50 : 50 beam splitter which can be used as a component to implement a Mach-Zehnder interferometer. In Bloch sphere representation, the two species would be both lined towards the same pole.

B. Two-mode squeezer limit

If almost all the atoms in the two species are circulating in opposite directions modes $\hat{b}_1 \simeq \hat{b}_1^\dagger \simeq \sqrt{N_1}$ and $\hat{a}_2 \simeq \hat{a}_2^\dagger \simeq \sqrt{N_2}$ (in Bloch sphere representation, the two species would be both lined towards opposite poles), we have

$$\hat{H}_Q \approx N_1 \hat{a}_1^\dagger \hat{a}_1 + N_2 \hat{b}_2^\dagger \hat{b}_2 + \frac{1}{2}(N_1 + N_2) + \sqrt{N_1 N_2} (\hat{a}_1 \hat{b}_2 + \hat{a}_1^\dagger \hat{b}_2^\dagger). \quad (24)$$

Here the last term creates or destroys pairs of quanta in analogy to a parametric amplifier or a two-mode squeezer [45]. This element could be used, e.g., to create highly entangled states of the atomic samples with metrological applications. If one can vary the sign of the nonlinearity, one can build a SU(1,1) interferometer [46] as a sequence of steps where first a squeezing Hamiltonian is applied, then a phase shifter (the phase of which is to be determined), and finally an

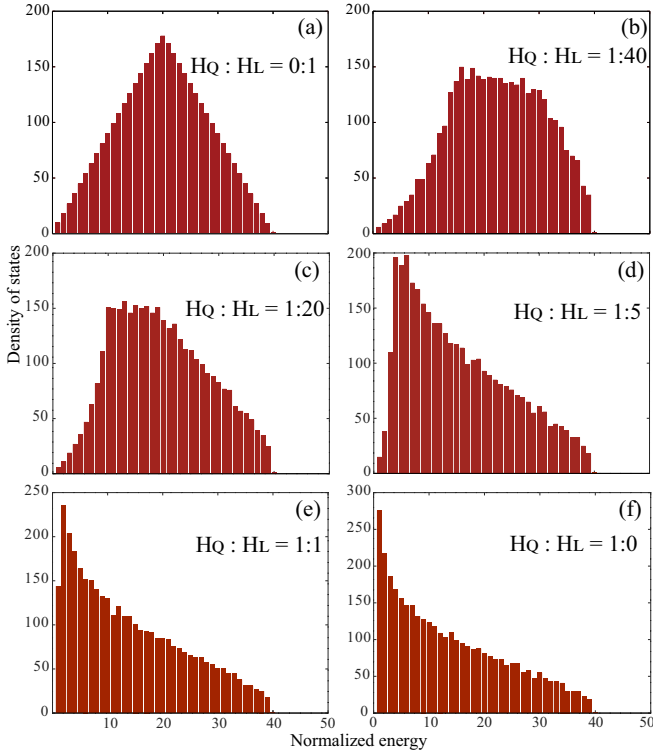


FIG. 6. The distribution of energies is shown for the case of $N_1 = N_2 = 59$, as we vary the full Hamiltonian in Eq. (9) from being purely linear, $\hat{H} = \hat{H}_L$, in panel (a) to being purely quadratic $\hat{H} = \hat{H}_Q$ in panel (f). In the linear limit, we assume $\hat{H}_L = (\hat{J}_{x1} - \hat{J}_{x2})$ in Eq. (9), corresponding to a rotating ring with no azimuthal lattice.

unsqueezing Hamiltonian, which will require the opposite sign of the nonlinearity χ_{12} .

VII. DENSITY OF STATES

While the variation of the spectrum in ranging from the linear to the quadratic Hamiltonian showed the degeneracy structure of the ground state, other significant differences can be identified by examining the density of states. In Fig. 6, we plot the distribution of the energies as we adjust from the purely linear to the purely quadratic Hamiltonian. There is a marked difference. In the linear limit, the distribution shows a peak in the middle of the spectrum stemming from the fact that the energy eigenstates are the Dicke states of the two species with flat energy spectra. Combining these two individual spectra yields the largest number of possibilities for the middle value of the energy. In the purely quadratic limit, the distribution is strongly skewed towards the ground state. This follows from the energy function as shown in Fig. 5 where large areas of parameters z_+ and n correspond to small energy values. There is a gradual morphing of the distribution as we transition from one limit to the other. The disappearance of the peak and occurrence of a monotonously decreasing spectrum is suggestive of an excited-state quantum phase transition in the system [47].

VIII. EXPERIMENTAL FEASIBILITY

We now confirm the feasibility of our model and its assumptions in the context of experimental parameters currently available. The analytical results for the quadratic Hamiltonian assume the interatomic interactions strengths to be equal: $\chi_1 = \chi_2 = \chi_{12}$. This is not an essential or limiting assumption, as we will further elaborate on later in this section. However, regimes close to equal strengths can be accessed for example with the hyperfine states $|F, m_F\rangle = |1, -1\rangle$ and $|2, 1\rangle$ for ^{87}Rb , taken as the two species, for which all the scattering lengths are close to $a = 100 a_0$ [43]. We will assume this value for our estimates of experimental parameters.

We consider a ring of major radius $R \approx 10 \mu\text{m}$ such as used in a recent experiment with ring traps [2], and a strong transverse trap frequency of $\omega_r = 2\pi \times 2000 \text{ Hz}$ along the minor radius r , noting that such kilohertz range confinement is typical for creating quasi-1D systems [48]. Assuming ^{87}Rb , our energy unit set by the lowest circulating mode evaluates to $\hbar\omega_1 = 3.85 \times 10^{-34} \text{ J}$, with corresponding frequency unit $\omega_1 = 3.65 \text{ Hz}$. This yields an interaction energy scale of $\hbar\chi = a\hbar\omega_r/(\pi R) = 1.10\hbar\omega_1$, and puts the system definitely in the 1D regime with the ratio of the azimuthal to transverse energy scale being $\omega_1/\omega_r \simeq 3 \times 10^{-4}$.

If we take the lattice to have periodicity $q = 5$, the system can be easily maintained in the two-mode regime: As discussed in Sec. II, for the interatomic interactions we ignored scattering to $\pm 3q$, which for our value of q will imply a minimal energy gap between the relevant modes of $\hbar\omega_1[(3q)^2 - q^2]/2 = 100\hbar\omega_1$ far larger than the interaction energy $\hbar\chi$ estimated above. By Bloch's theorem, for $q = \pm 5$ the energetically closest modes the lattice can couple are $n = 0$ and ± 10 so that the minimal energy gap separating $\pm q$ modal subspace from other possible coupled modes is $\hbar\omega_1(q^2/2) = 12.5\hbar\omega_1$. Using a separate independently tunable potential to generate it, the lattice can be made sufficiently weak to satisfy this condition. In general current technology allows for all of the parameters to be adjusted substantially, but this underscores the general experimental feasibility of our results.

With two species there can be phase separation, with Thomas-Fermi estimates that neglect the kinetic energy, setting the criterion $\Delta\chi = \chi_{12} - \sqrt{\chi_1\chi_2}$ that separates regimes of miscibility ($\Delta\chi < 0$) and immiscibility ($\Delta\chi > 0$) [49]. In our model the two species need to maintain interspecies interaction, implying reasonable overlap of the densities of the two species. We provide a brief analysis to show that this remains valid within our assumptions, by computing the density-density correlation as a function $\Delta\chi$. Defining the two-mode density operator for each species $i = 1, 2$,

$$\hat{\rho}_i(s) \equiv \frac{1}{2\pi} (\hat{a}_i^\dagger e^{-is} + \hat{b}_i^\dagger e^{is})(\hat{a}_i e^{is} + \hat{b}_i e^{-is}), \quad (25)$$

the overlap of the species can be gauged by

$$\hat{\mathcal{O}} \equiv \int_{2\pi} \langle \hat{\rho}_1 \hat{\rho}_2 \rangle ds = \frac{N_1 N_2}{2\pi} + \frac{1}{\pi} (\hat{J}_{x1} \hat{J}_{x2} + \hat{J}_{y1} \hat{J}_{y2}), \quad (26)$$

where we have assumed length unit R and the expectation is taken with respect to the ground state of the quadratic part of the Hamiltonian in Eq. (8), but setting $\chi_1 = \chi_2 = \chi$ so that $\Delta\chi = \chi_{12} - \chi$. The maximum and minimum eigenvalues

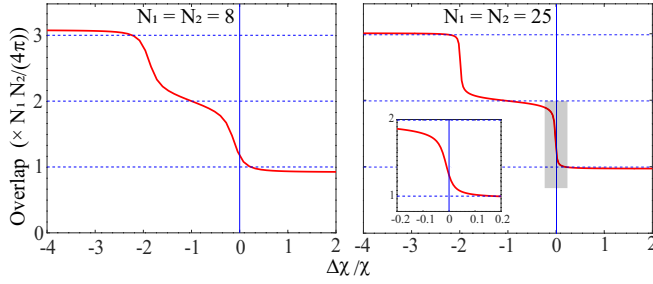


FIG. 7. Overlap of the densities of the two atomic species plotted in units of $N_1 N_2 / (4\pi)$, with the solid red line showing exact quantum values, and the dashed horizontal blue lines marking the semiclassical estimates for limiting cases of the interspecies interaction χ_{12} , in ascending order: strongly repulsive, zero, and strongly attractive. The inset highlights that the transition in the neighborhood of the critical point $\Delta\chi = 0$ (marked by vertical blue line) is gradual over a relevant regime.

of the operator $\hat{J}_{x1}\hat{J}_{x2} + \hat{J}_{y1}\hat{J}_{y2}$ determine through the above expression the range in which the overlap of the two species can occur. We benchmark our results with a semiclassical approximation of the density operator in Eq. (25):

$$\begin{aligned} \bar{\mathcal{O}} &= \int_{2\pi} \rho_1 \rho_2 ds, \\ \rho_i(s) &= \frac{N_k}{2\pi} [1 + \mathcal{V}_i \cos(2s + \gamma_i)], \end{aligned} \quad (27)$$

where $\mathcal{V}_k \in [0, 1]$ is a measure of visibility of the interference pattern and γ_i is a phase determining the angular orientation of the pattern. For pure states, the case $\mathcal{V}_i = 0$ corresponds to a uniform density for all atoms orbiting in the same direction, whereas $\mathcal{V}_i = 1$ corresponds to a standing wave where half of the atoms orbit clockwise and the other half orbit counter-clockwise.

Three special cases are relevant.

(i) For *strongly repulsive* interaction, $\Delta\chi/\chi \gg 1$, two species form pronounced standing waves where the density minima of one species coincide with the maxima of the other, such that $\gamma_1 - \gamma_2 = \pi$.

(ii) For a *strongly attractive* interaction, $\Delta\chi < 0$ and $|\Delta\chi/\chi| \gg 1$, the interference patterns of the two species will tend to maximally overlap with $\gamma_1 - \gamma_2 = 0$.

(iii) For *vanishing* interaction $\chi_{12} = 0$, or $\Delta\chi/\chi = -1$, each species will have a uniform distribution with $\mathcal{V}_i = 0$. These cases yield

$$\begin{aligned} \chi_{12} \gg \chi : \bar{\mathcal{O}} &= \frac{N_1 N_2}{4\pi}, \\ \chi_{12} \ll -|\chi| : \bar{\mathcal{O}} &= \frac{3N_1 N_2}{4\pi}, \\ \chi_{12} = 0 : \bar{\mathcal{O}} &= \frac{N_1 N_2}{2\pi}. \end{aligned} \quad (28)$$

We plot our results in Fig. 7 for two different numbers of particles $N_1 = N_2 = 8$ and 25, with the exact calculations using Eq. (26) plotted in solid red lines, with horizontal dashed blue lines marking the three semiclassical limiting cases above. One can see that with increasing particle number

quantum calculations approach the semiclassical estimates in the corresponding limits.

What is relevant for us is that even though there is clearly a transition in the density correlation at $\Delta\chi = 0$ when all the interaction strengths are identical, the overlap remains finite and nonvanishing, set by the lowest semiclassical values in Eq. (28). This means that our assumption of equal nonlinear strengths is not a constraint at all, although that regime can be experimentally accessed and allows for analytical calculations. The primary physical impact will be a reduction in the degree of entanglement possible in proportion to any decline in the interspecies interaction strength. The inset in Fig. 7 also shows that in a small ring where the kinetic energy cannot necessarily be neglected, the transition is not sharp at $\Delta\chi = 0$, but gradual over a relevant range of variation of about $|\Delta\chi/\chi| \leq 20\%$. Finally, we should note that these calculations here and similar ones in much of the literature are done in the absence of a lattice, but there have been several experiments such as in Ref. [48] with two interacting species of atoms without phase separation being a limiting obstacle, and the lattice can have an impact in suppressing phase separation.

IX. CONCLUSIONS AND OUTLOOK

Our analysis here shows that two species of ultracold atoms in a ring trap can provide a viable alternate platform to examine nontrivial quantum features that rely on entanglement. The model can be viewed as two Lipkin-Meshkov-Glick systems coupled by two bilinear terms formed as products of components of collective spin operators. Here we mapped out the static and spectral properties as a necessary preliminary to examining the dynamical phenomena that can exploit the entanglement, which we are actively exploring in our continuing work. Among such applications, we already identified here certain limiting cases that can be adapted for interferometry as well as for generating two-mode squeezing.

One relevant way to use the entangled states in this system would be to implement quantum teleportation [50], particularly the transition regime from small to large atomic numbers where the continuous variable limit for teleportation [51] can be expected. With regards to all such quantum phenomena involving entangled states, the ring system offers the opportunity to study them in the context of motional states encapsulated in circulating modes in the ring, rather than with internal states like spin typically utilized in the majority of platforms studied. This can facilitate a natural scaling up of the system size and the time scales involved, that can help better understand some of the most intriguing aspects of quantum mechanics.

ACKNOWLEDGMENTS

This work was supported by Czech Science Foundation Grant No. 20-27994S for T.O. and by NSF Grants No. PHY-2011767 and No. PHY-2309025 for K.K.D. We thank Prof. Dominik Schneble and Allison Brattley for valuable discussions.

- [1] L. de Broglie, A tentative theory of light quanta, *Phil. Mag.* **47**, 446 (1924).
- [2] A. Ramanathan, K. C. Wright, S. R. Muniz, M. Zelan, W. T. Hill, C. J. Lobb, K. Helmerson, W. D. Phillips, and G. K. Campbell, Superflow in a toroidal Bose-Einstein condensate: An atom circuit with a tunable weak link, *Phys. Rev. Lett.* **106**, 130401 (2011).
- [3] K. C. Wright, R. B. Blakestad, C. J. Lobb, W. D. Phillips, and G. K. Campbell, Driving phase slips in a superfluid atom circuit with a rotating weak link, *Phys. Rev. Lett.* **110**, 025302 (2013).
- [4] C. Brooks, A. Brattley, and K. K. Das, Rotation-sensitive quench and revival of coherent oscillations in a ring lattice, *Phys. Rev. A* **103**, 013322 (2021).
- [5] I. Bloch, J. Dalibard, and W. Zwerger, Many-body physics with ultracold gases, *Rev. Mod. Phys.* **80**, 885 (2008).
- [6] H. Huang and K. K. Das, Effects of a rotating periodic lattice on coherent quantum states in a ring topology: The case of positive nonlinearity, *Phys. Rev. A* **104**, 053320 (2021).
- [7] M. Kitagawa and M. Ueda, Squeezed spin states, *Phys. Rev. A* **47**, 5138 (1993).
- [8] S. Gupta, K. W. Murch, K. L. Moore, T. P. Purdy, and D. M. Stamper-Kurn, Bose-Einstein condensation in a circular waveguide, *Phys. Rev. Lett.* **95**, 143201 (2005).
- [9] A. S. Arnold, C. S. Garvie, and E. Riis, Large magnetic storage ring for Bose-Einstein condensates, *Phys. Rev. A* **73**, 041606(R) (2006).
- [10] J. A. Sauer, M. D. Barrett, and M. S. Chapman, Storage ring for neutral atoms, *Phys. Rev. Lett.* **87**, 270401 (2001).
- [11] K. Henderson, C. Ryu, C. MacCormick, and M. G. Boshier, Experimental demonstration of painting arbitrary and dynamic potentials for Bose-Einstein condensates, *New J. Phys.* **11**, 043030 (2009).
- [12] B. E. Sherlock, M. Gildemeister, E. Owen, E. Nugent, and C. J. Foot, Time-averaged adiabatic ring potential for ultracold atoms, *Phys. Rev. A* **83**, 043408 (2011).
- [13] J. G. Lee and W. T. Hill, Spatial shaping for generating arbitrary optical dipole traps for ultracold degenerate gases, *Rev. Sci. Instrum.* **85**, 103106 (2014).
- [14] A. Turpin, J. Polo, Y. V. Loiko, J. Küber, F. Schmalz, T. K. Kalkandjiev, V. Ahufinger, G. Birkel, and J. Mompert, Blue-detuned optical ring trap for Bose-Einstein condensates based on conical refraction, *Opt. Express* **23**, 1638 (2015).
- [15] T. A. Bell, J. A. P. Glidden, L. Humbert, M. W. J. Bromley, S. A. Haine, M. J. Davis, T. W. Neely, M. A. Baker, and H. Rubinsztein-Dunlop, Bose-Einstein condensation in large time-averaged optical ring potentials, *New J. Phys.* **18**, 035003 (2016).
- [16] M. Meister, S. Arnold, D. Moll, M. Eckart, E. Kajari, M. A. Efremov, R. Walser, and W. P. Schleich, *Efficient Description of Bose-Einstein Condensates in Time-Dependent Rotating Traps*, edited by E. Arimondo, C. C. Lin, and S. F. Yelin, *Advances In Atomic, Molecular, and Optical Physics*, Vol. 66 (Academic Press, 2017) pp. 375–438.
- [17] S. Franke-Arnold, J. Leach, M. J. Padgett, V. E. Lembessis, D. Ellinas, A. J. Wright, J. M. Girkin, P. Öhberg, and A. S. Arnold, Optical ferris wheel for ultracold atoms, *Opt. Express* **15**, 8619 (2007).
- [18] R. Zambrini and S. M. Barnett, Angular momentum of multi-mode and polarization patterns, *Opt. Express* **15**, 15214 (2007).
- [19] F. Jendrzejewski, S. Eckel, N. Murray, C. Lanier, M. Edwards, C. J. Lobb, and G. K. Campbell, Resistive flow in a weakly interacting Bose-Einstein condensate, *Phys. Rev. Lett.* **113**, 045305 (2014).
- [20] S. Eckel, J. G. Lee, F. Jendrzejewski, N. Murray, C. W. Clark, C. J. Lobb, M. Phillips, W. D. Edwards, and G. K. Campbell, Hysteresis in a quantized superfluid ‘atomtronic’ circuit, *Nature (London)* **506**, 200 (2014).
- [21] D. Aghamalyan, M. Cominotti, M. Rizzi, D. Rossini, F. Hekking, A. Minguzzi, L.-C. Kwek, and L. Amico, Coherent superposition of current flows in an atomtronic quantum interference device, *New J. Phys.* **17**, 045023 (2015).
- [22] D. Aghamalyan, L. Amico, and L. C. Kwek, Effective dynamics of cold atoms flowing in two ring-shaped optical potentials with tunable tunneling, *Phys. Rev. A* **88**, 063627 (2013).
- [23] F. Pinheiro and A. F. R. de Toledo Piza, Delocalization and superfluidity of ultracold bosonic atoms in a ring lattice, *J. Phys. B* **46**, 205303 (2013).
- [24] I. I. Satija, Carlos L. Pando L., and E. Tiesinga, Soliton dynamics of an atomic spinor condensate on a ring lattice, *Phys. Rev. A* **87**, 033608 (2013).
- [25] M. Maik, P. Buonsante, A. Vezzani, and J. Zakrzewski, Dipolar bosons on an optical lattice ring, *Phys. Rev. A* **84**, 053615 (2011).
- [26] K. Hettiarachchilage, V. G. Rousseau, K.-M. Tam, M. Jarrell, and J. Moreno, Phase diagram of the Bose-Hubbard model on a ring-shaped lattice with tunable weak links, *Phys. Rev. A* **87**, 051607(R) (2013).
- [27] H. M. Cataldo and D. M. Jezek, Bose-Hubbard model in a ring-shaped optical lattice with high filling factors, *Phys. Rev. A* **84**, 013602 (2011).
- [28] D. M. Jezek and H. M. Cataldo, Winding-number dependence of Bose-Einstein condensates in a ring-shaped lattice, *Phys. Rev. A* **83**, 013629 (2011).
- [29] G. Arwas and D. Cohen, Chaos and two-level dynamics of the atomtronic quantum interference device, *New J. Phys.* **18**, 015007 (2016).
- [30] G. Arwas, D. Cohen, F. Hekking, and A. Minguzzi, Resonant persistent currents for ultracold bosons on a lattice ring, *Phys. Rev. A* **96**, 063616 (2017).
- [31] J. Polo, P. Naldesi, A. Minguzzi, and L. Amico, Exact results for persistent currents of two bosons in a ring lattice, *Phys. Rev. A* **101**, 043418 (2020).
- [32] A. Richaud and V. Penna, Pathway toward the formation of supermixed states in ultracold boson mixtures loaded in ring lattices, *Phys. Rev. A* **100**, 013609 (2019).
- [33] A. Muñoz Mateo, V. Delgado, M. Guilleumas, R. Mayol, and J. Brand, Nonlinear waves of Bose-Einstein condensates in rotating ring-lattice potentials, *Phys. Rev. A* **99**, 023630 (2019).
- [34] M. Nigro, P. Capuzzi, and D. M. Jezek, Blocked populations in ring-shaped optical lattices, *Phys. Rev. A* **98**, 063622 (2018).
- [35] T. Opatrný, M. Kolář, and K. K. Das, Spin squeezing by tensor twisting and Lipkin-Meshkov-Glick dynamics in a toroidal Bose-Einstein condensate with spatially modulated nonlinearity, *Phys. Rev. A* **91**, 053612 (2015).
- [36] M. Kolář, T. Opatrný, and K. K. Das, Criticality and spin squeezing in the rotational dynamics of a Bose-Einstein condensate on a ring lattice, *Phys. Rev. A* **92**, 043630 (2015).

- [37] H. J. Lipkin, N. Meshkov, and A. Glick, Validity of many-body approximation methods for a solvable model-I, II, III, *Nucl. Phys.* **62**, 188 (1965).
- [38] F. Lingua, A. Richaud, and V. Penna, Residual entropy and critical behavior of two interacting boson species in a double well, *Entropy* **20**, 84 (2018).
- [39] C. Gross, T. Zibold, E. Nicklas, J. Estève, and M. K. Oberthaler, Nonlinear atom interferometer surpasses classical precision limit, *Nature (London)* **464**, 1165 (2010).
- [40] M. F. Riedel, P. Böhi, Y. Li, T. W. Hänsch, A. Sinatra, and P. Treutlein, Atom-chip-based generation of entanglement for quantum metrology, *Nature (London)* **464**, 1170 (2010).
- [41] T. OpatrŇy, Quasicontinuous-variable quantum computation with collective spins in multipath interferometers, *Phys. Rev. Lett.* **119**, 010502 (2017).
- [42] A. M. Childs, Y. Su, M. C. Tran, N. Wiebe, and S. Zhu, Theory of Trotter error with commutator scaling, *Phys. Rev. X* **11**, 011020 (2021).
- [43] M. Egorov, B. Opanchuk, P. Drummond, B. V. Hall, P. Hannaford, and A. I. Sidorov, Measurement of s -wave scattering lengths in a two-component Bose-Einstein condensate, *Phys. Rev. A* **87**, 053614 (2013).
- [44] C. H. Bennett, H. J. Bernstein, S. Popescu, and B. Schumacher, Concentrating partial entanglement by local operations, *Phys. Rev. A* **53**, 2046 (1996).
- [45] U. Leonhardt, *Essential Quantum Optics: From Quantum Measurements to Black Holes* (Cambridge University, New York, 2010), pp. 92–134.
- [46] B. Yurke, S. L. McCall, and J. R. Klauder, SU(2) and SU(1,1) interferometers, *Phys. Rev. A* **33**, 4033 (1986).
- [47] P. Cejnar, P. Stránský, M. Macek, and M. Kloc, Excited-state quantum phase transitions, *J. Phys. A* **54**, 133001 (2021).
- [48] J. Kwon, Y. Kim, A. Lanuza, and D. Schneble, Formation of matter-wave polaritons in an optical lattice, *Nat. Phys.* **18**, 657 (2022).
- [49] C. J. Pethick and H. Smith, *Bose-Einstein Condensation in Dilute Gases*, 2nd ed. (Cambridge University, Cambridge, England, 2002).
- [50] C. H. Bennett, G. Brassard, C. Crépeau, R. Jozsa, A. Peres, and W. K. Wootters, Teleporting an unknown quantum state via dual classical and Einstein-Podolsky-Rosen channels, *Phys. Rev. Lett.* **70**, 1895 (1993).
- [51] S. L. Braunstein and H. J. Kimble, Teleportation of continuous quantum variables, *Phys. Rev. Lett.* **80**, 869 (1998).